SANDIA REPORT
SAND2018-4080
Unlimited Release
Printed April, 2018

Recent research on stishovite: Hugoniot and partial release Z experiments and DFT EOS calculations

Michael D. Furnish[1] Luke Shulenburger[2], Michael Desjarlais[3], and Yingwei Fei[4]

[1]Dynamical Material Properties Department 1646
[2]HEDP Theory Department 1641
[3]Pulsed Power Sciences Center 1600
[4]Carnegie Institution of Washington

Prepared by
Sandia National Laboratories
Albuquerque, New Mexico 87185 and Livermore, California 94550

Sandia National Laboratories is a multimission laboratory managed and operated by National Technology and Engineering Solutions of Sandia LLC, a wholly owned subsidiary of Honeywell International Inc. for the U.S. Department of Energy's National Nuclear Security Administration under contract DE-NA0003525.

Sandia National Laboratories

Issued by Sandia National Laboratories, operated for the United States Department of Energy by Sandia Corporation.

SAND2018-4080
Unlimited Release
Printed April, 2018

Recent research on stishovite: Hugoniot and partial release Z experiments and DFT EOS calculations

Michael D. Furnish[1] Luke Shulenburger[2], Michael Desjarlais[3], and Yingwei Fei[4]

[1]Dynamical Material Properties Department 1646
[2]HEDP Theory Department 1641
[3]Pulsed Power Sciences Center 1600

Sandia National Laboratories
P.O. Box 5800
Albuquerque NM 87185-1195

[4] Geophysical Laboratory
Carnegie Institution of Washington
5251 Broad Branch Road, NW
Washington, DC 20015

Abstract

We have conducted a series of ride-along experiments on the Z facility to ascertain the Hugoniot of silica centered in the stishovite phase over a range 0.4 - 1.0 TPa, together with partial release states produced at the interface between the sample and a fused silica window. The stishovite samples were synthesized in a large-volume multi-anvil press at 15 GPa and 1773 K, with an initial density of 4.29 gm/cc. The new Z experiments on stishovite fill in a gap between gas gun experiments and NIF experiments. The states are compared with the Hugoniots of quartz and fused silica for inferences as to EOS. They are generally consistent with Sesame 7360 predictions. Sound speed constraints from these data are discussed. The new Hugoniot data cross over the melting curve of stishovite; together with the partial-release data and predictions from density-functional theory modeling, they provide insights into the properties of solid and liquid under extreme conditions. These data are fundamentally important for understanding the interior of silicate-based super-Earths.

Acknowledgments

As with any program relying on ride-along slots for Z experiments, we owe thanks to the program sponsoring those experiments (here, DOE Campaign 2), and to the many people required to assemble and execute a set of shots on Z. Included in this are Jim Williams and Lynn Twyeffort (designers), the Target Fab group, Marcus Knudson (key in the conduct of the first two shots), and the Carnegie personnel who helped synthesize the stishovite samples. Sandia National Laboratories is a multimission laboratory managed and operated by National Technology and Engineering Solutions of Sandia LLC, a wholly owned subsidiary of Honeywell International Inc., for the U.S. Department of Energy's National Nuclear Security Administration under contract DE-NA0003525.

Table of Contents

Figures

Tables

Recent research on stishovite: Hugoniot and partial release Z experiments and DFT EOS calculations

1.0 Introduction and Background

Stishovite is a tetragonal high-pressure polymorph of SiO_2, and is believed to be a key component of the earth's lower mantle and of parts of other rocky planets. In this structure, each silicon atom is surrounded by 6 oxygen atoms in an octahedral arrangement; stishovite is thus markedly different from other polymorphs of SiO_2. Two phase diagrams of this material are shown in Fig. 1.1

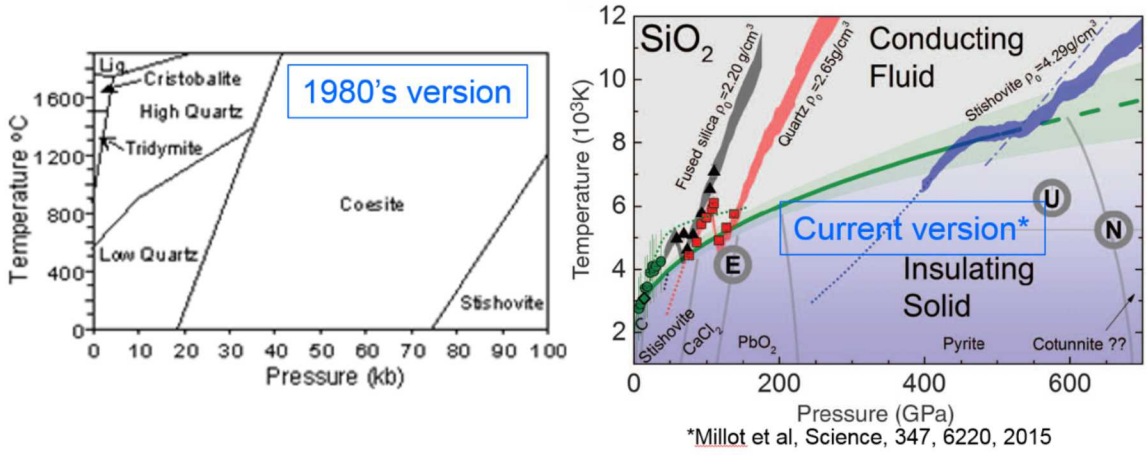

Figure 1.1. Phase diagrams of stishovite. 100 kb = 10 GPa.

Key questions to be investigated in the present study include the shock equation-of-state and partial release behavior. Due to the experimental design, sound speed at the Hugoniot (useful for tying data to seismic properties of the lower mantle) is not available from these experiments.

An early attempt to obtain this information used a two-stage light gas gun (Furnish and Ito, 1995) with samples synthesized in a belt-press. Methods available at that time were not well suited to the small sample sizes used (3 mm diameter and 0.5 – 0.8 mm thick) and had very large uncertainties. A more recent study by Millot, et al (2015) used a transparent stishovite single crystal sample and several polycrystalline samples on OMEGA laser-driven experiments to obtain the data shown in Fig. 1.2. Although that study was published after the current experiments were underway, the current work is interesting in that it provides (1) shock data within the large gap below 1 TPa (10 MBar) in the laser data set, and (2) partial release data which may offer useful information about phase transitions in this material.

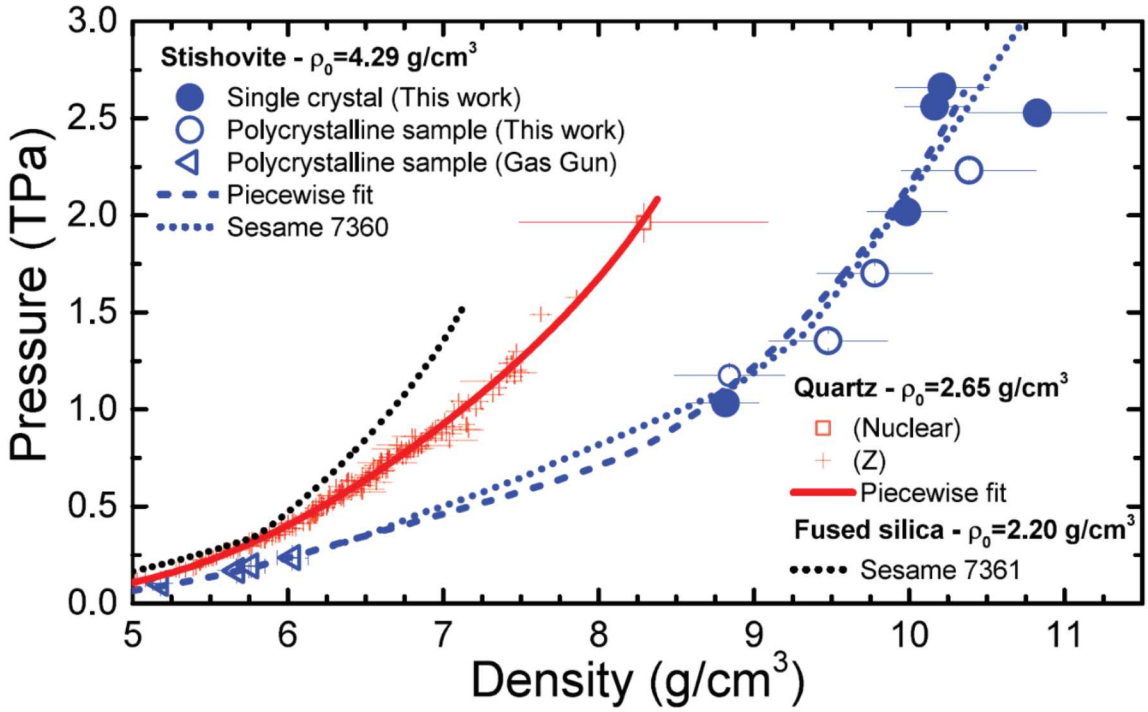

Figure 1.2. Results of study by Millot et al, 2015.

2.0 Experimental Configuration

2.1 Notional description and EOS calculation methods

This study was comprised of 5 experiments on the Z machine, as enumerated in Table 2.1. Each was a two-sided coaxial flyer plate experiment (described later) impacting aluminum flyer plates into the samples.

Table 2.1. List of Z experiments (short names for shots in parentheses).

Shot number	Hardware Set	Date	Impactor Velocities
Z2826 (2)	A0483A	6/30/2015	14.4, 15.85
Z2828 (3)	A0483B	7/2/2015	12.25, 13.5
Z2902 (4)	A0542A	1/26/16	20.15, 21.55
Z3001 (5)	A0559	9/16/16	18.66, 20.0
Z3035 (6)	A0574	12/12/16	24.02, 25.2

The stishovite sample was directly impacted by the flyer, and was supported and backed by a Z-cut alpha quartz (Z-quartz") window. There were 2 – 3 points on each flyer plate whose velocity was measured by VISAR during launch and impact on Z-quartz windows; these waveforms were used to determine the impact time and velocity on the fronts of the stishovite samples. For each case, the impact produces a sufficiently strong shock in the quartz window to give a reflective shock front whose velocity can be measured by VISAR [Knudson and Desjarlais, 2009]. From this measurement and the sample Hugoniot state, the partially released state in the sample could be deduced.

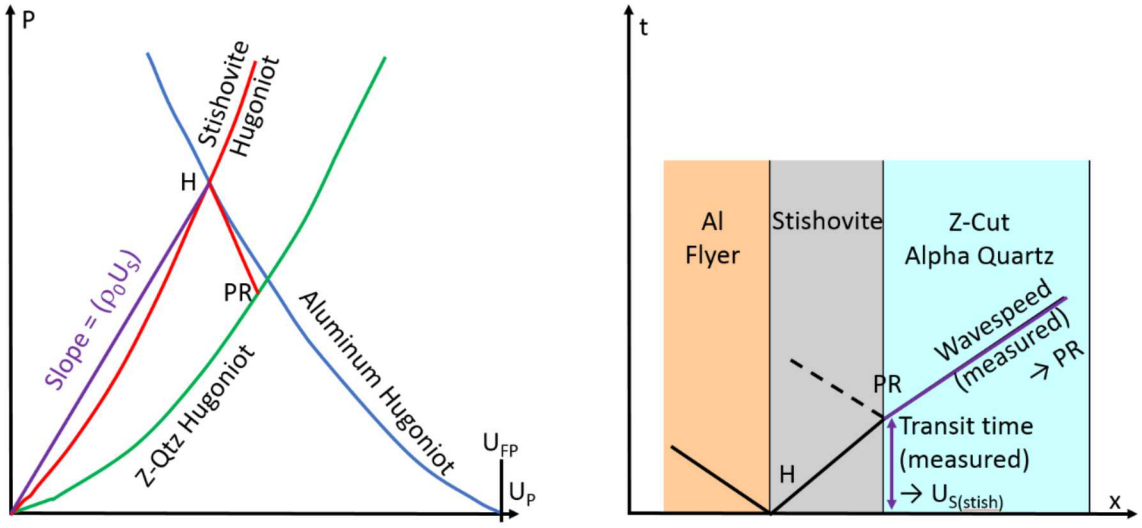

Figure 2.1. Schematic of impact configuration. (Left) Pressure vs. particle velocity. H = Hugoniot state; PR = partial release; U_{FP} = Flyer plate velocity. (Right) time vs. position. Derivation of Hugoniot and partial release state is shown schematically.

Calculating the sample Hugoniot state requires measuring the shock transit time through the sample (therefore knowing the wavespeed), determined by subtracting the impact time from the shock arrival time at the sample window interface. The most significant uncertainty is this impact time, which must be calculated from the impact

times at the adjacent spots (with slight corrections for differences in flyer plate flight distances).

The sample experiences a release when the shock wave enters the quartz window. The pressure and particle velocity of the partially released state is calculated from the measured wavespeed in the Z-quartz (which must be divided by the index of refraction of α-quartz, which is 1.547 at the 532 nm wavelength used in the present experiments.). The quartz parameters are taken as $\rho_0 = 2.65$ gm/cc, $a = 6.26$ km/s, $b = 1.2$, $c = 2.56$ and $d = 0.37$ s/km, with the quartz shock velocity expressed as $U_s = a + bu_p - cu_p \exp(-d\, u_p)$. If steady-wave assumptions about this release wave are applied, the partially-released density and the wavespeed of the release wave are available. However, the steady-wave assumptions are not strictly correct. Errors due to this are not detailed in the present report.

Uncertainties are propagated via Monte Carlo methods (see §3.3).

2.2 Hardware

The present discussion focusses on the liquid portion of the test; those considerations drove design decisions that affected the context of the stishovite samples.

The clear liquid experiments were designed as shown in Fig. 2.2. This setup, known as a coaxial liquid cell configuration, includes two panels on opposite sides of the cathode stalk (a tongue-depressor shaped aluminum piece affixed to the Z cathode magnetically insulated transmission lines, or MITLs). Aluminum flyer plates 1 mm thick and 29 mm wide are set on opposite sides of the cathode stalk, separated from the stalk by 1.0 and 1.4 mm (south and north, respectively). During the experiment, electrical current flows up the cathode stalk and down the flyer plates. Lorentz forces accelerate the flyer plates across the gaps into the respective panels. Z current pulse shapes, A/K gaps and flight distances are chosen so that the plates accelerate smoothly without shockup, impact the respective panels at approximately the same time, and preserve sufficient thickness during launch to impose a supported shock which does not attenuate during passage through the sample.

The two panels afford two slightly (10 – 20%) different impact velocities, with correspondingly different shock amplitudes generated in the samples. This is due to differing anode/cathode (A/K) gaps and flight distances.

Because the samples are transparent, the VISAR records from the probes viewing these samples afford an abundance of information: (1) the acceleration record of the flyer plate, (2) the quartz shock wave speed in the buffer, (3) the time at which the shock enters the sample, (4) the time-dependent shock wave speed of the wave crossing the sample (measured directly by the VISAR), (5) the time the shock enters the quartz window, and (6) the shock wave speed (hence stress amplitude) in the window.

This experimental setup also allows for a second pair of experiments on the bottom section of the panels, as well as another probe on each panel viewing the flyer plate. These locations were used for samples of geophysical interest.

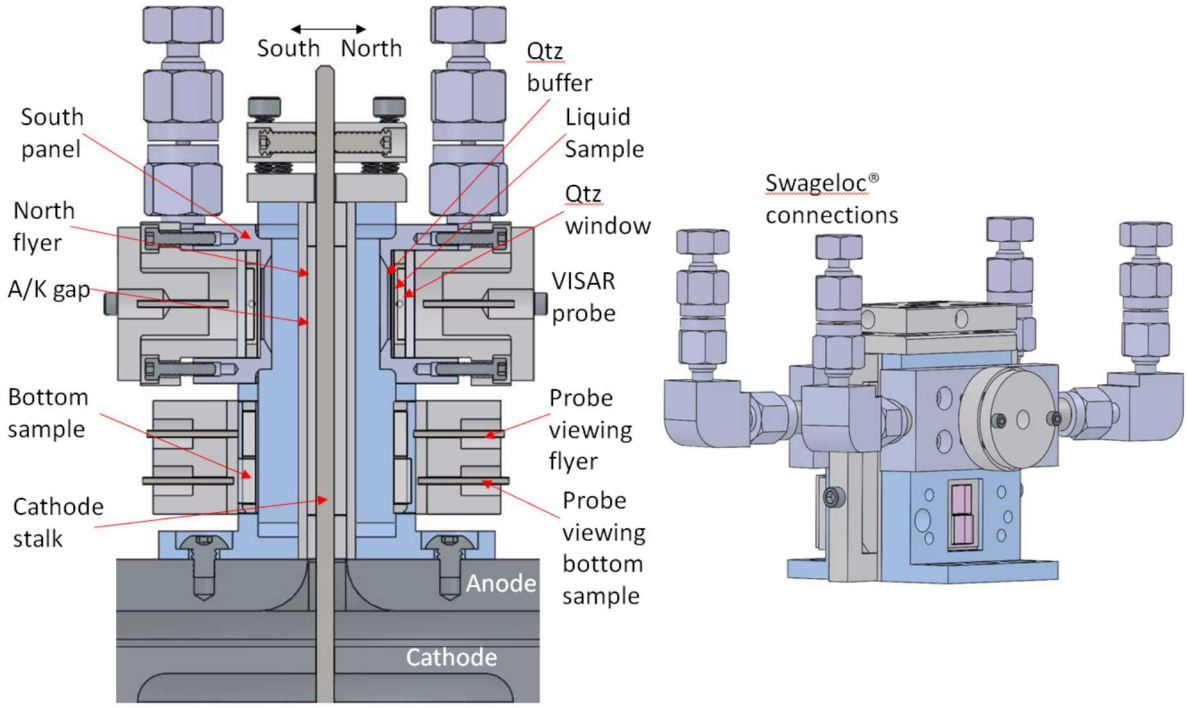

Figure 2.2. Z hardware for the neat liquid experiments (transparent samples).

For the experiments with an opaque liquid mixture, it was necessary to add an additional VISAR probe on each panel to view the flyer plate adjacent to the liquid sample (Fig. 2.3). As well, the sample chamber thicknesses were increased from 0.4 mm to 1.0 mm due inhomogeneity of the liquid mixtures. The aluminum flyer plate thickness was increased from 1.0 to 1.2 mm to ensure the thickness at impact would be enough so the rarefaction from the flyer rear surface would not overtake the shock in the sample.

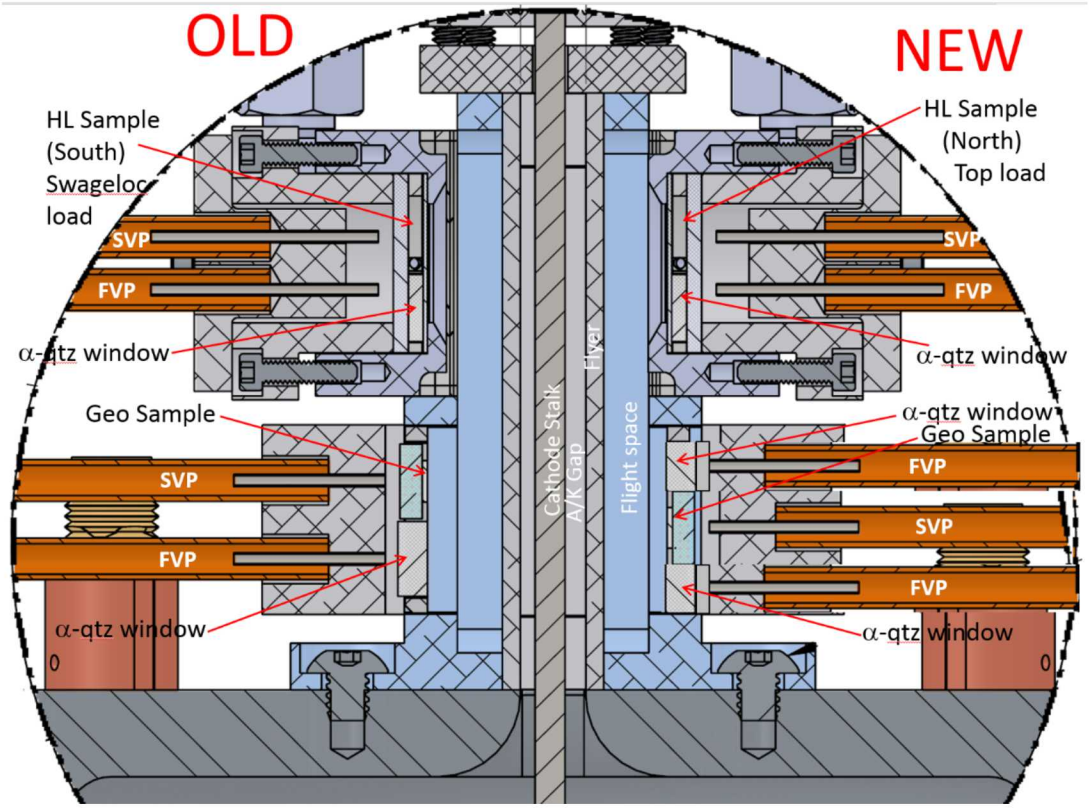

Figure 2.3. Configuration for opaque liquid samples (2 – 7 except 4). FVP = flyer-viewing probe; SVP = sample-viewing probe. Upper samples are Hydroliquid; lower are ride-along stishovite (SiO_2) samples except Z3107 (which tested bridgmanite, or $MgSiO_3$). "Old" configuration was used for both panels for all shots except 5, 6, 7 (Z3001, 3035, 3107).

For purposes of interpreting the stishovite data, the panel maps in Fig. 2.4 suffice. A key point is that the flight distances to impact the stishovite samples and the adjacent window(s) were measured prior to shot, but those to impact the liquid cell were not. Therefore it was necessary to integrate the flyer plate motion data to deduce these distances and therefore the flyer shape during launch.

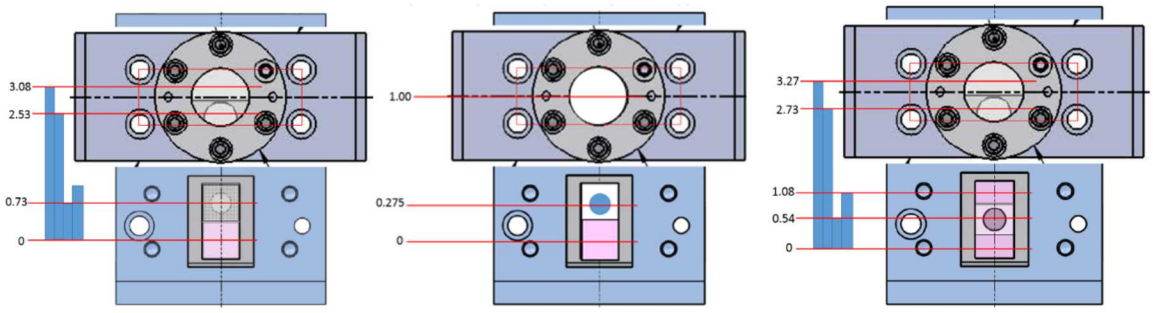

Figure 2.4. Panel maps. (Left) Plan view of each of the two panels for shots 2, 3, with the stishovite samples at 0.73 units and flyer-viewing probes at 0 and 2.53 units. (Middle) Shot 4 plan view, similar to shots 2, 3 except that the upper flyer-viewing probe is through the transparent liquid sample at 1.00 units, and the stishovite is at 0.275 units. (Right) Plan view for shots 5, 6, with flyer viewing probes at 0, 1.08 and 2.73 units and the stishovite sample at 0.54 units. A shot 7 exists with the same configuration, but included bridgmanite instead of stishovite.

2.3 Diagnostics

The two probes viewing the liquid samples each used 7 fibers: 1 for sending light, 5 for receiving light to be sent to the VISAR systems, and one for the passive SVS (Streak Visible Spectroscopy) system. The other six probes (three per panel) each used 4-fiber configurations, 1 for sending light and 3 to return Doppler-shifted light to the VISAR systems. VISAR signals were recorded for 5 μs, timed to place the motion of interest near the center of the record.

Two 19-beam VISAR interferometers, manufactured by National Security Technologies (Special Technologies Laboratory), were set up to include velocity-per-fringe settings ranging from 277.71 m/s up to 2.2895 km/s. 28 of these channels were used on each of the present shots.

Timing was accomplished by recording light returns during a test run in which the laser light at the source is momentarily electronically blocked, giving a 1.5 ns FWHM dip in the measured light levels, and accounting for the known portions of the 2-way transit to the target.

Impact time on the Z-quartz buffer was established by extrapolating the impact times observed on the flyer-viewing VISAR probes to the sample location. Uncertainties in this process were typically ~ 0.25 – 1.0 ns.

2.4 Sample Synthesis

The stishovite samples were synthesized in a large-volume octahedral cell at the Carnegie Institution of Washington at a pressure of 15 GPA and a temperature of 1500 C. The typical grain size was ~4 microns, and the phase was confirmed by Raman spectroscopy. The sample diameters were 2.8 mm.

3.0 Results

3.1 Flyer performance

Flyer plate launches were smooth throughout the experiment, and well-diagnosed. The North Bottom flyer plate measurement for Z2826 (shot 2) is shown in Fig. 3.1. (only one of the three sets of VISAR fringe records is shown). The signature of impact was clear for all flyer plate measurements, whether using LiF or Z-cut α-quartz windows. This record is typical of the flyer plate launches in this series.

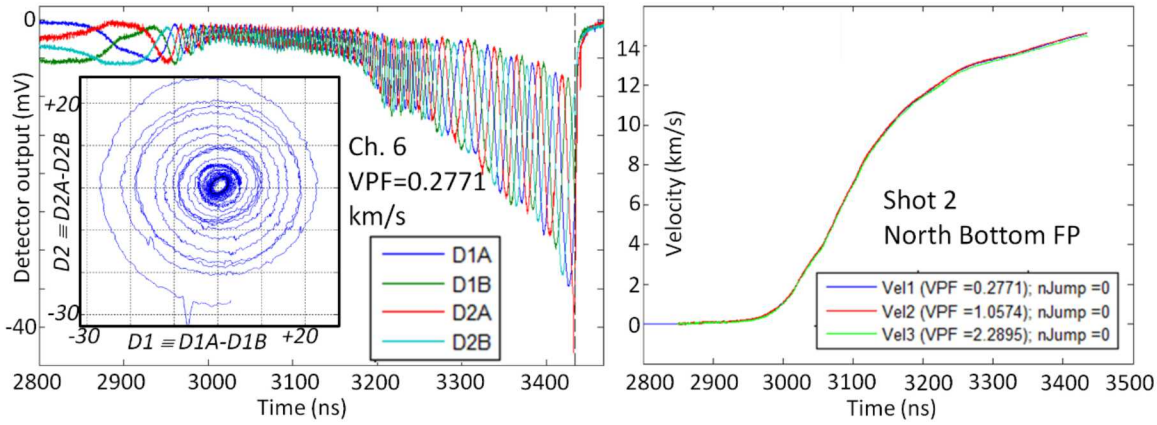

Figure 3.1. VISAR records for Z2826 North Bottom flyer plate. (Left) Fringe record and inset Lissajous pattern for Channel 6 (VFP = 0.2771 km/s). (Right) Plot of all three velocity records for this flyer plate measurement.

Flyer plate measurements with Z-cut α-quartz windows showed fringe activity after impact corresponding to the shock wave propagating through the window. We have not analyzed these signatures in detail. For LiF windows (e.g. the record shown in Fig. 4.1), the light was quickly extinguished after impact.

Critical to the interpretation of impact time is the question of impact planarity. Only shots 5 and 6 had more than 2 points monitored on each flyer plate; results for these are shown in Fig. 3.2. The stishovite sample is located at a position of 0.54. These times are corrected to constant flight distance (see Section 2.2).

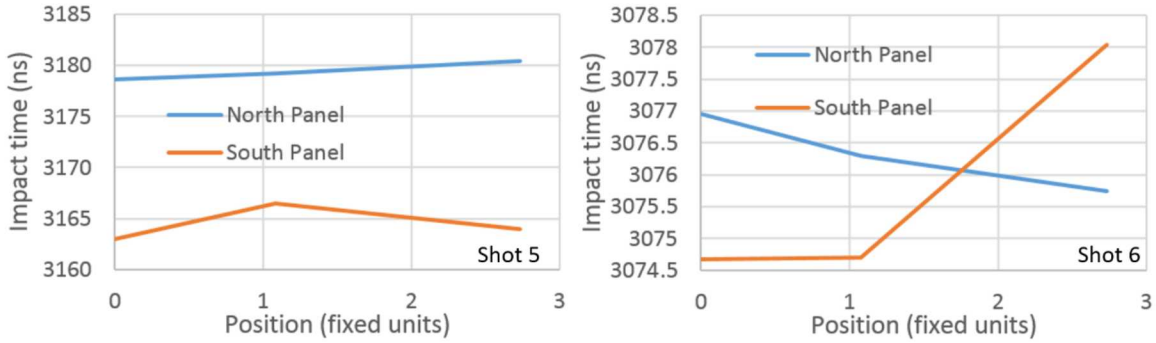

Figure 3.2. Impact planarity for shots 5 and 6, corrected to constant flight distance.

3.2 Representative velocimetry results

Consider the velocimetry data from the north panel liquid probe in shot 6 (Z3035), shown in Fig. 3.2. It provides a time-of-arrival of the shock at the back of the stishovite sample and a measurement of the velocity of the shock into the Z-cut α-quartz window. The initial arrival is determined by first deflection of the fringes, and is measured to ~0.25 ns. Cross-timing with the adjacent flyer-viewing signals provides impact information under the sample, as discussed elsewhere.

The velocity of the shock in the Z-cut α-quartz window (Fig. 3.3 bottom right) provides a measure of the reshock state in the sample. To obtain this velocity, a large number of fringe jumps are required (see Dolan [2006]). Choosing the correct number of fringes requires bringing the velocity amplitudes into agreement, together with physics sanity checks to be discussed in §3.3. Following the initial arrival and a plateau, the wave begins to decelerate as the release from the back of the flyer plate overtakes the shock front. However, this cannot be used directly to determine the sound speed at the Hugoniot state because the thickness of the flyer at time of impact is not well known (estimated as 0.2 – 0.4 mm after thinning by the Z current during launch).

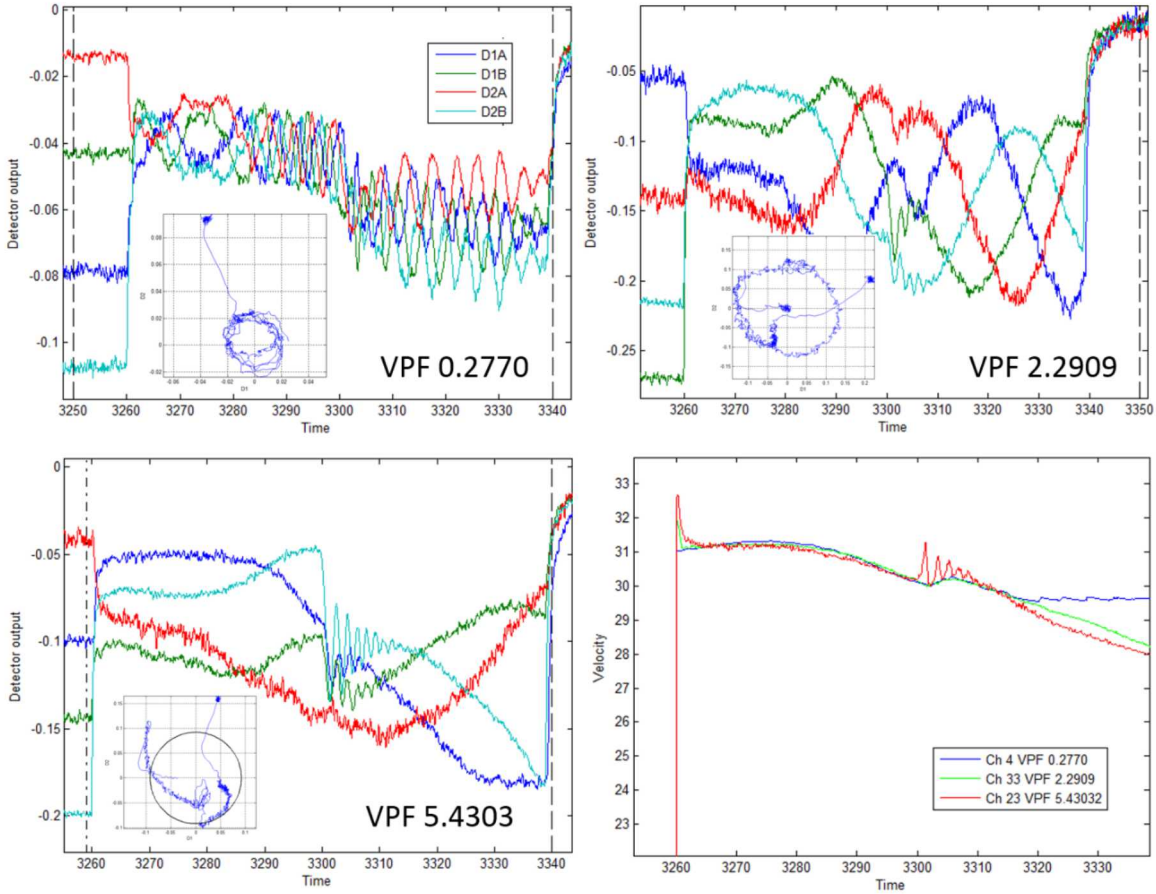

Figure 3.3. VISAR records for Z2828 North Stishovite probe. (Left) Fringe record and inset Lissajous pattern for Channel 24 (VFP = 1.0455 km/s). (Right) Plot of all five velocity records for this probe. measurement.

3.3 Stishovite Hugoniots and partial release states

In the present experiments, the liquid cells are attached to the two panels of the coaxial configuration just before shot time, and the positions of these cells relative to the flyer plate are never explicitly measured. For most similar Z experiments, the flight distances to all target components are carefully measured in the Target Fabrication laboratory ahead of final assembly. Therefore, the interpretation of these shots included a careful integration of flyer motion to deduce these flight distances to impact.

For all shots except Z3107 (aka Shot 7), monolithic stishovite samples were placed in the bottom sample locations. The observables are listed in Table 3.1, and the resulting Hugoniot and reshock values are listed in Table 3.2 and plotted in Fig. 3.4. In Table 3.2, the primary observable quantities are the shock velocity for the Hugoniot and the particle velocity (from the post-arrival wavespeed) for the partial release state.

Table 3.1. Input parameters for the stishovite samples. U_{FP} is the impact velocity. Post-arrival wavespeed is the apparent shock velocity in the quartz window downstream of the sample, and must be divided by the index of refraction of the Z-cut quartz window, $n_{Qtz} = 1.547$.

Test	Stishovite Thickness mm	Initial Density gm/cc	Impact Velocity km/s	Impact time μs	Breakout Time μs	Post-arrival wavespeed km/s
2 North	0.631(1)	4.26(2)	14.62(5)	3.3680(5)	3.4037(3)	23.40(20)
2 South	0.658(1)	4.28(2)	16.00(5)	3.3818(5)	3.4221(3)	24.50(20)
3 North	0.369(1)	4.31(2)	12.25(5)	2.8060(5)	2.8299(4)	20.80(15)
3 South	0.425(1)	4.34(2)	13.50(5)	2.8055(5)	2.8330(3)	22.10(15)
4 North	0.679(1)	4.30(2)	20.15(5)	2.6803(5)	2.7176(4)	27.50(30)
4 South	0.616(1)	4.27(2)	21.55(5)	2.6824(5)	2.7137(4)	28.60(30)
5 North	0.369(1)	4.29(2)	18.70(5)	3.1789(5)	3.1996(4)	25.70(30)
5 South	0.452(1)	4.29(2)	19.96(5)	3.1633(5)	3.1877(4)	26.75(30)
6 North	0.319(1)	4.29(2)	23.91(5)	3.0746(5)	3.0896(3)	30.64(30)
6 South	0.795(1)	4.29(2)	25.39(5)	3.0737(5)	3.1111(2)	31.35(30)

Table 3.2. Hugoniot and release values for the stishovite samples.

Test	Hugoniot					Partial Release			
	Pressure (GPa)	Shock Velocity (km/s)	Particle Velocity (km/s)	Density (gm/cm^3)	Strain	Pressure (GPa)	Density (gm/cm^3)	Particle Velocity* (km/s)	Release Velocity‡ (km/s)
2 North	426(4)	17.69(29)	5.67(5)	6.27(8)	0.320(8)	330(6)	4.39(20)	8.23(9)	6.0(7)
2 South	462(4)	16.35(24)	6.61(5)	7.19(11)	0.404(9)	366(7)	5.38(23)	8.72(9)	6.4(8)
3 North	316(5)	15.49(42)	4.74(7)	6.22(11)	0.307(12)	253(4)	4.05(22)	7.09(7)	4.4(5)
3 South	361(4)	15.46(33)	5.38(6)	6.66(11)	0.348(11)	290(4)	4.50(22)	7.65(7)	4.7(5)
4 North	668(7)	18.21(30)	8.53(7)	8.10(17)	0.469(11)	476(12)	7.31(23)	10.11(14)	15.3(2.5)
4 South	760(9)	19.68(38)	9.04(8)	7.91(19)	0.460(13)	521(12)	7.29(22)	10.64(14)	19.3(3.1)
5 North	597(10)	17.84(53)	7.80(11)	7.64(26)	0.438(19)	408(11)	7.01(27)	9.27(14)	17.2(3.2)
5 South	665(10)	18.49(46)	8.38(10)	7.86(24)	0.454(16)	447(12)	7.35(25)	9.76(14)	20.6(3.8)
6 North	913(18)	21.18(70)	10.05(15)	8.19(37)	0.475(23)	610(14)	7.67(35)	11.62(15)	24.1(4.6)
6 South	992(7)	21.28(24)	10.87(6)	8.77(15)	0.511(8)	643(14)	8.50(16)	11.98(15)	36.9(7.2)

* Referenced to the laboratory frame; ‡ Eulerian wavespeed (i.e. in space of material in Hugoniot state)

The uncertainties for the Hugoniot are mostly due to the reported uncertainty in the

shock transit time ($t_{(Back\ surface)} - t_{(Impact)}$); those for the reshock, to the uncertainty in the post-arrival wavespeed (the shock velocity in the quartz window).

Strictly speaking, the last column in Table 3.2 (a sort of averaged release wave speed) is inaccurate because it is computed using steady-wave assumptions, and we do not expect those to apply here. However, it may offer a loose estimate of the sound speed at the Hugoniot. For a proper measurement of that quantity, a two-layer flyer plate (e.g. copper on aluminum) should be used in conjunction with several sample thicknesses. That construction was not used here because the liquid sample measurements required a well-supported shock.

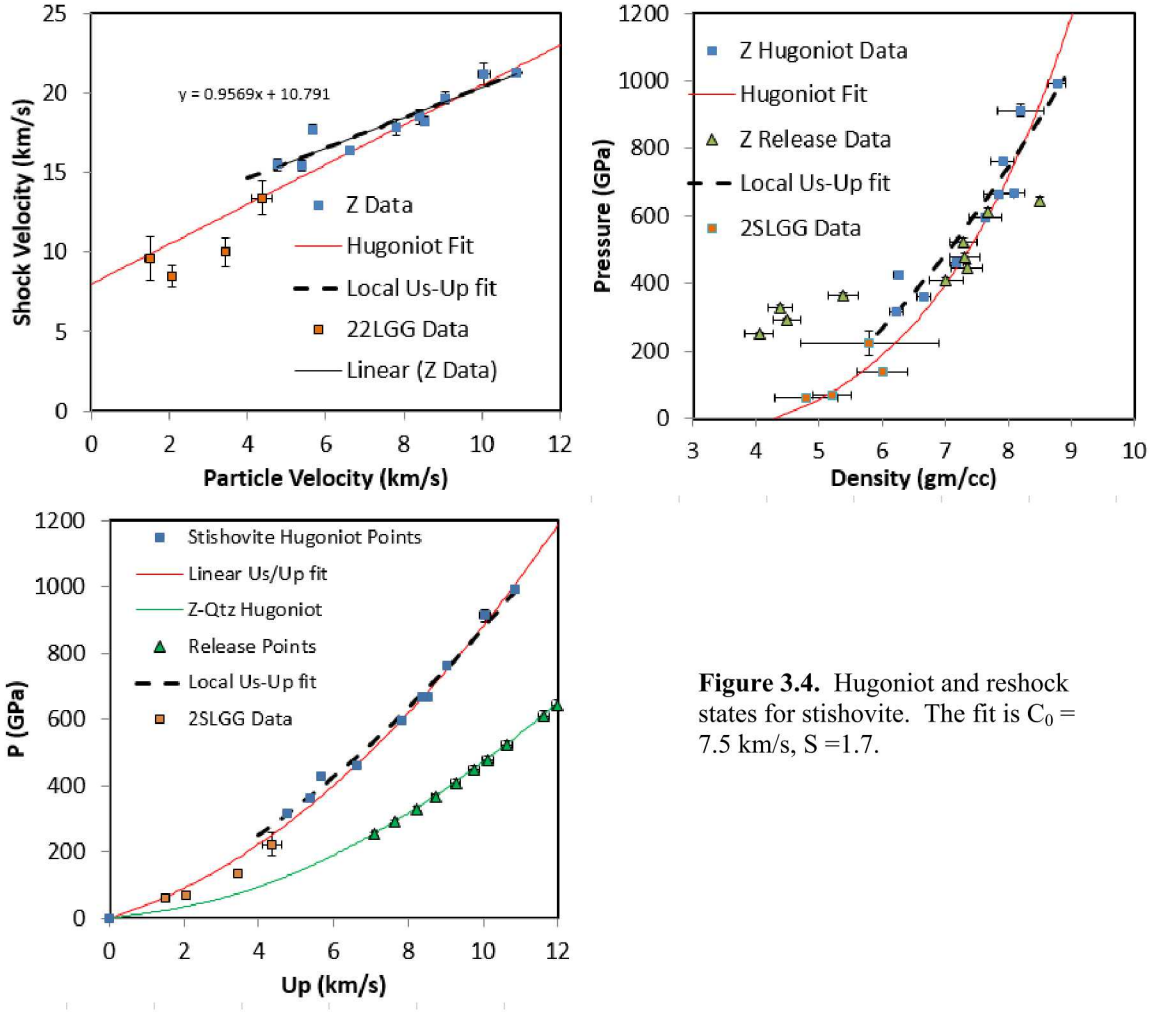

Figure 3.4. Hugoniot and reshock states for stishovite. The fit is C_0 = 7.5 km/s, S =1.7.

The Hugoniot and partially release states may be plotted in the pressure-density space against other data to give a scientific context, as in Fig. 3.5. The Hugoniot data appear to lie sensibly on the interpolation of the Millot (2015) data; as well, the partial release data suggest a change is occurring at the ~0.5 TPa level (refreeze?).

An earlier analysis of these data did not use the proper flyer plate shapes because it assumed a nominal flight distance for the liquid cell samples. The results of that analysis, shown in Fig. 3.6, are clearly above the expected curve in pressure-density space.

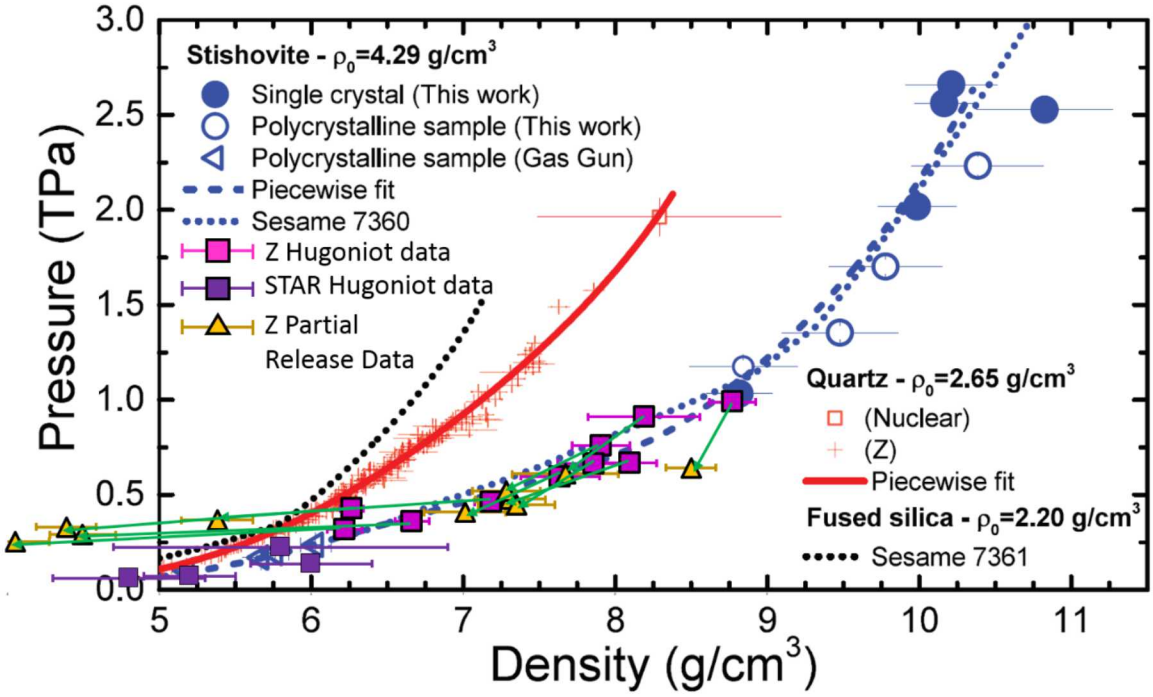

Figure 3.5. Stishovite data, plotted over figure from Millot et al, 2015.

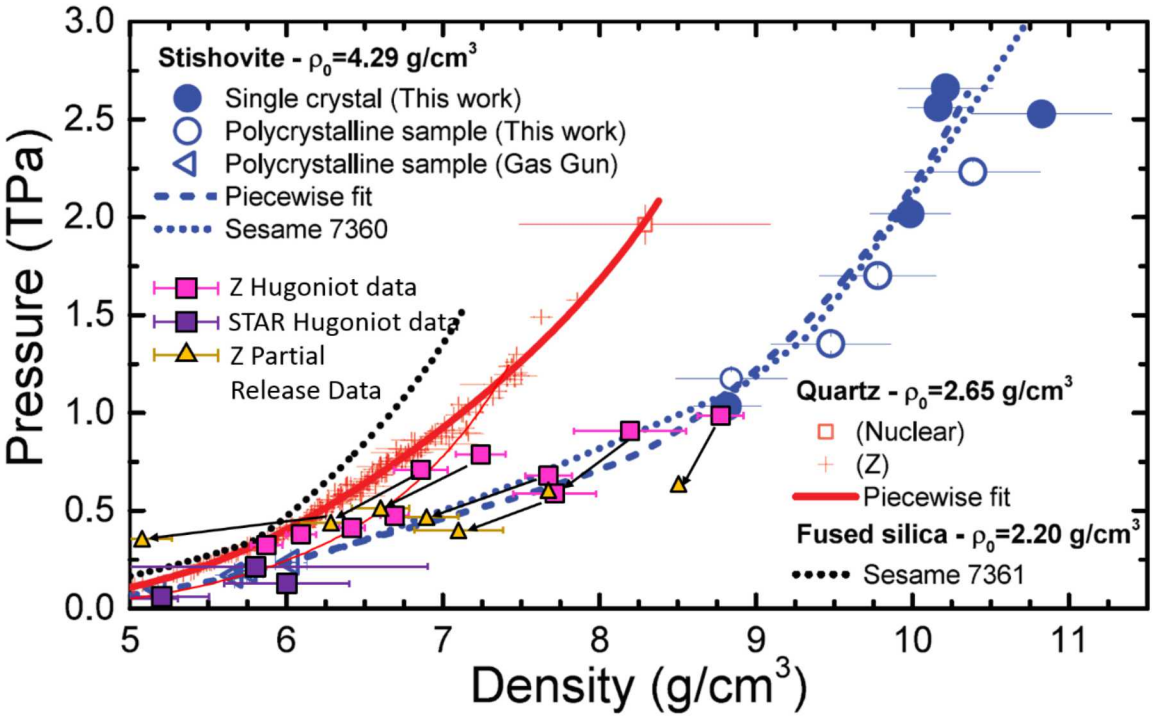

Figure 3.6. Stishovite EOS, assuming nominal liquid-cell flight distances. These EOS data are not credible.

4.0 Density Functional Theory modeling

We have modeled the silica system using DFT molecular dynamics with VASP and two different functionals to predict these Hugoniots. The results are shown in Fig. 4.1. LDA is the local density approximation. PBEsol is a form of generalized gradient approximation (GGA) optimized for densely packed solids and their surfaces (Perdew, *et al*., 2008). The pyrite and liquid calculations assume those structures. In general, we consider the agreement of these calculations with experiment to be satisfactory.

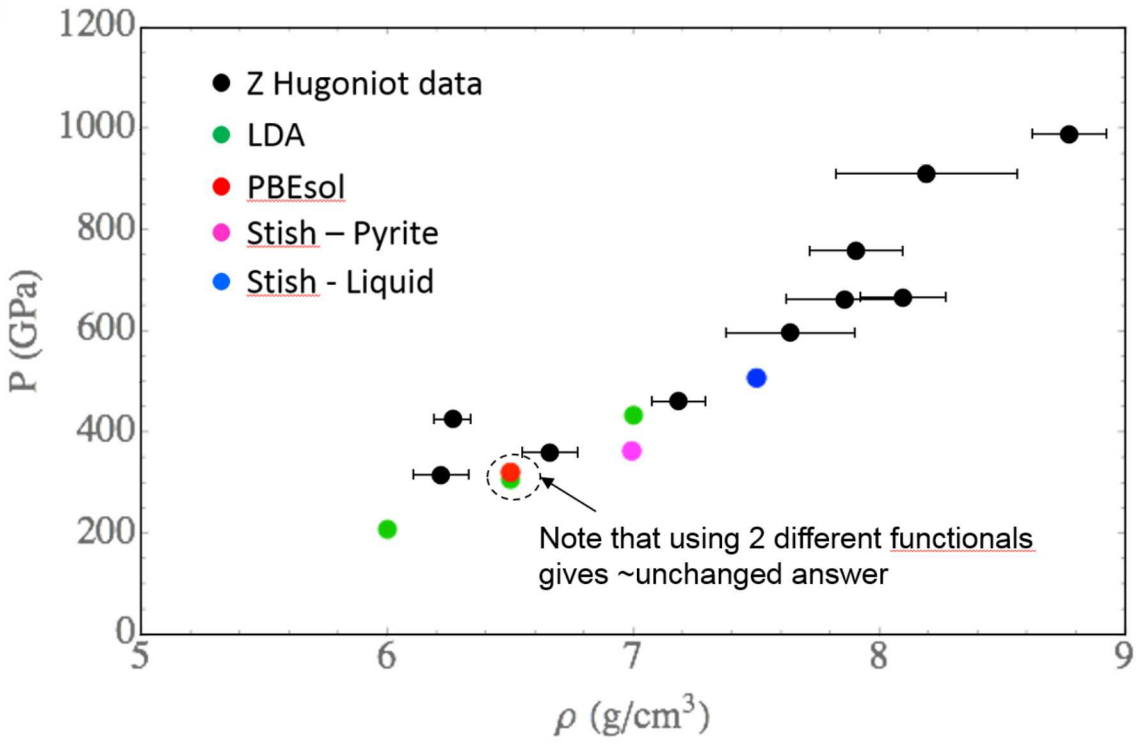

Figure 4.1. Present stishovite Hugoniot data, compared with DFT models.

5.0 Afterword

The measurement of shock transit times in opaque samples carries the difficulty that the impact time must be inferred from nearby probes, an inference sensitive to the shape of the flyer plate. Such an effort succeeds or fails depending on the proper interpretation of many details. An accurate knowledge of flight distances to impact on the various components of the target is key. For these experiments, the liquid cell positions were not measured after final mounting due to the logistics of late-time loading. Therefore the most accurate determination of flight distances was obtained by integrating the flyer motion until impact on the flyer-viewing probes. When the actual flight distances were used, the results made sense.

It is possible the results could be further improved (and the uncertainties tightened) using a method suggest by C. Seagle after M. Knudson. Relative timing of similar features on different fringe records can often be determined accurately by timeshifting one trace until the features overlay (facilitated by scaling the traces vertically so the features are of similar amplitude).

It would be useful to include stishovite samples on future experiments using layered impactors to better measure sound speeds at the Hugoniot state.

References

Dolan, D. H. Foundations of VISAR analysis, Sandia National Laboratories report, SAND2006-1950.

Knudson, M. D. and Desjarlais, M.P., Shock compression of quartz to 1.6 TPa: Redefining a pressure standard, Phys. Rev. Lett. 103, 225501, 2009.

Knudson, M. D. and Desjarlais, M.P., Adiabatic release measurements in α-quartz between 300 and 120 GPa: Characterization of α-quartz as a shock standard in the multimegabar regime, Phys. Rev. Lett. 103, 225501, 2009.

Perdew, J. P., Ruzsinszky, A., Csonka, G. I., Vydrov, O. A., Scuseria, G. E., Constantin, L. A., Zhou, X., and Burke, K., Restoring the Density-Gradient Expansion for Exchange in Solids and Surfaces, Phys. Rev. Lett., 100, 13406, 2008.

Millot, M., et al, Shock compression of stishovite and melting of silica at planetary interior conditions, Science, 347, 6220, 2015.

Distribution

Internal:

MS 1195	Dept. 1646	M. D. Furnish (electronic copy)
MS 1195	Dept. 1646	C. T. Seagle (electronic copy)
MS 1195	Dept. 1646	S. Root (electronic copy)
MS 0899	Dept., 9536	Technical Library (electronic copy)

External:

Y. Fei
Geophysical Laboratory
Carnegie Institution of Washington
5251 Broad Branch Road, NW
Washington, DC 20015


Sandia National Laboratories